Classical Energy Deposition and Refraction in Spherical and Planar Laser Fusion Targets

James E. Howard

November 1976

UWFDM-188

FUSION TECHNOLOGY INSTITUTE

UNIVERSITY OF WISCONSIN

MADISON WISCONSIN

Classical Energy Deposition and Refraction in Spherical and Planar Laser Fusion Targets

James E. Howard

Fusion Technology Institute
University of Wisconsin
1500 Engineering Drive
Madison, WI 53706

http://fti.neep.wisc.edu

November 1976

UWFDM-188

"LEGAL NOTICE"

"This work was prepared by the University of Wisconsin as an account of work sponsored by the Electric Power Research Institute, Inc. ("EPRI"). Neither EPRI, members of EPRI, the University of Wisconsin, nor any person acting on behalf of either:

"a. Makes any warranty or representation, express or implied, with respect to the accuracy, completeness, or usefulness of the information contained in this report, or that the use of any information, apparatus, method, or process disclosed in this report may not infringe privately owned rights; or

"b. Assumes any liabilities with respect to the use of, or for damages resulting from the use of, any information, apparatus, method or process disclosed in this report."

Classical Energy Deposition and Refraction in Spherical and Planar Laser Fusion Targets

James E. Howard

UWFDM-188

ABSTRACT

Geometric optics is used to study classical absorption of laser light by inverse bremsstrahlung in plane and spherical isothermal plasmas. The absorption integral (optical thickness) and minimum point of the ray path are given in closed form for slab geometry, and as asymptotic series in the spherical case. The absorption is integrated over a spatial beam profile based on optimal illumination studies and used to define an effective angle of incidence. An expanding critical radius (the usual case) is found to significantly reduce the average angle of incidence. Implications for resonance absorption in reactor-size pellets are presented.

Contents

FIGURE CAPTIONS

FIG. 1. Ray path through a spherical plasma.

FIG. 2. Ray path through a planar plasma and corresponding exponential density profile.

FIG. 3. Displacement of ray at minimum point in slab geometry.

FIG. 4. Normalized absorption integral versus projected angle of incidence in spherical geometry for an exponential density profile, various scale heights.

FIG. 5. Target illumination for an ideal lens.

FIG. 6. Cubic exponential beam profile. A width parameter of about a = 0.7 produces uniform illumination for 12 or 20 beams.

FIG. 7. Integrated absorption for an ideal f/1.5 lens. The dashed curves correspond to a 50% expansion in critical radius.

FIG. 8. Effective angle of incidence for an ideal f/1.5 lens.

FIG. 9. Reduction of projected angle of incidence for an expanding critical radius.

FIG. 10. Integrated absorption for an ideal f/1.5 leans, with a 100% increase in critical radius.

FIG. 11. Effective angle of incidence for an ideal f/1.5 lens with a 50% increase in critical radius.

FIG. 12. Effective angle of incidence for an ideal f/1.5 lens with a 100% increase in critical radius.

FIG. 13. Integrated absorption for an ideal f/3.5 lens. The dashed curves correspond to a 50% increase in critical radius.

FIG. 14. Effective angle of incidence for an ideal f/3.5 lens.

FIG. 15. Effective angle of incidence for an ideal f/3.5 lens, with a 50% increase in critical radius.

FIG. 16. Effective angle of incidence for an ideal f/3.5 lens, with a 100% increase in critical radius.

FIG. 17. Curves of scale height versus angle of incidence for maximal resonance absorption.

1. Introduction

Economic operation of a laser fusion reactor depends critically on the amount of laser energy absorbed by the target material. It is well known that collisional absorption decreases rapidly with increasing electron temperature and therefore some additional process, probably resonance absorption[1], is needed to account for the amount of absorption observed experimentally[2,3]. Nevertheless, in many cases a substantial fraction of the total absorption may still be attributed to inverse bremsstrahlung and must be included in numerical simulations of resonance absorption[4].

In this paper we shall study linear collisional absorption by means of geometrical optics, which applies whenever the refractive index of the plasma does not change appreciably in a distance of one wavelength. Even at normal incidence, when the ray penetrates to the critical surface, it can be shown that geometric optics gives the correct absorption to within a few percent, except for long laser wavelengths and high-Z materials.[5] For spherically symmetric isothermal plasmas the absorption integral along a ray path can be reduced to a simple radial integral depending only on the density scale height and angle of incidence. This integral is performed in closed form in slab geometry, and asymptotically for small scale heights and angles of incidence in the spherical case.

Besides reducing the total absorption, refraction at oblique incidence also affects the distribution of energy within the corona[6]. Thus, an optical system designed to give uniform illumination at the critical radius (where the bulk of absorption occurs) may have to take into consideration the varying refraction of individual rays. In section 3 handy formulas are derived for ray displacements in terms of the density scale height

and angle of incidence in plane geometry, which approximates the sensitive initial phase in illuminating spherical targets. The reason for this sensitivity is the Rayleigh-Taylor instability[7].

Both theoretical studies[8] and numerical simulations[9] indicate that if catastrophic growth of the Rayleigh-Taylor instability is to be avoided, about 90% optical uniformity must be maintained at early times. Optimal illumination studies[10] show that better uniformity usually means larger angles of incidence as beams are overlapped. Thus, a certain amount of uniformity must be sacrificed in favor of smaller angles of incidence, to avoid excessive refractive loss of energy. In order to quantify this trade-off we have calculated the net absorption for an ideal illumination system, integrated over a spatial beam profile based on the aforementioned optimal illumination studies. The results of section 4 show an encouraging insensitivity to the maximum angle of incidence, due to the concentration of energy near the beam axis. However, the effective (weighted average) angle of incidence turns out to exceed the range where resonance absorption is expected to be strongest.

A possible mechanism for reducing the effective angle of incidence is the expansion of the critical surface as laser energy is absorbed. Numerical simulations of pellet implosions over a wide variety of pulse shapes and pellet sizes[11] predict an increase of 50-100% in critical radius by the time the maximum laser power arrives. In section 5 we model this expansion and calculate effective angles of incidence for a realistic beam profile. The results are encouraging for small or moderate size pellets. Unfortunately, as we show in section 6, it appears to be difficult to achieve the requisite conditions for resonance absorption in reactor-size pellets, even allowing for the expansion of the critical radius.

It should be noted that most of today's theory is motivated by the need to interpret current experiments using small targets. Reactor-grade pellets are much more massive, with the consequence that corona temperatures will be highly non-isothermal. Most present-day analyses of parametric instabilities ignore temperature gradients. For example, back-reflection due to stimulated Brillouin scattering,[12] a small effect in current experiments, may well be more pronounced in more massive targets.

2. Classical Absorption

In the classical picture, individual electrons gain energy by absorbing photons in the coulomb field on a nearby ion. For this reason, inverse bremsstrahlung is often referred to as "collisional", or "free-free" absorption. At low intensities, the classical and quantum-mechanical results are comparable, in which case the latter treatment might be termed "semiclassical". Both, however, are linear. The important nonlinear effects that come into play at intensities greater than about 10^{13} W/cm^2 will be discussed later.

Consider laser radiation obliquely incident on a spherically symmetric plasma, as illustrated in Fig. 1. The intensity along a ray path is given by

$$\Phi = \Phi_{IN} \exp\left(-\int_0^{\ell} \kappa(\ell) d\ell\right) \text{ W/cm}^2, \qquad (1)$$

where Φ_{IN} is the flux incident on the pellet and ℓ is distance measured along a ray. The quantum mechanical free-free absorption coefficient, corrected for spontaneous emission, can be written[13]

$$\kappa = \frac{4}{3}\left(\frac{2}{\pi m}\right)^{1/2} \left(\frac{e^6}{mc^3}\right)\lambda_L^2 \frac{Z_{eff}\, n_e^2}{N\theta_e^{3/2}} f(x) \text{ cm}^{-1} \qquad (2)$$

where, for a multi-species plasma,

$$Z_{eff} \equiv \frac{\langle Z^2 \rangle}{\langle Z \rangle}, \qquad (3)$$

$\theta_e = k\, T_e$, λ_L is the vacuum laser wavelength, N is the refractive index, and

$$f(x) \equiv \frac{\sinh x}{x} K_o(x), \qquad (4)$$

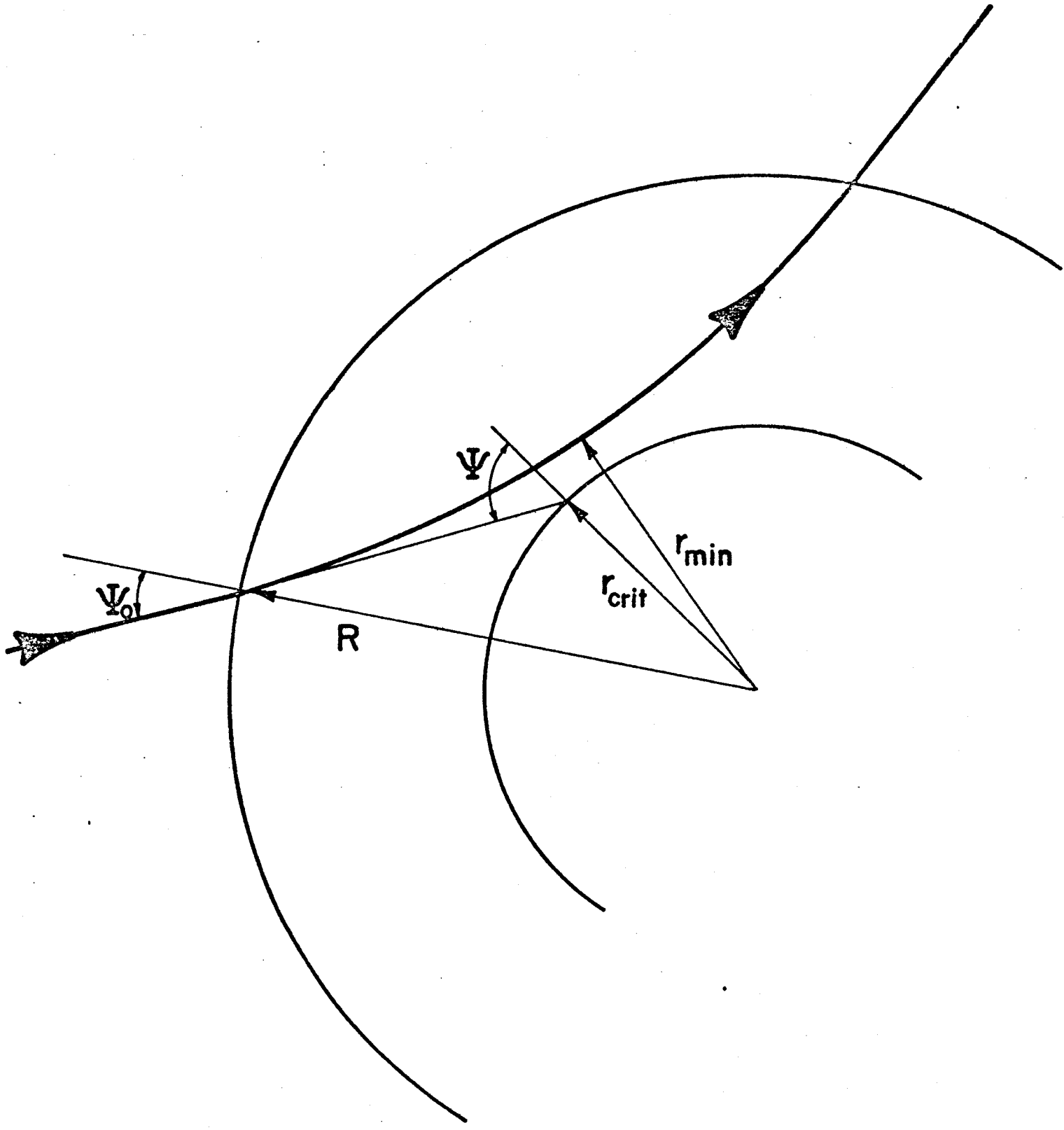

FIGURE 1

where $K_o(x)$ is the modified Bessel function of the second kind, and

$$x \equiv \frac{h\nu}{2\theta_e} . \tag{5}$$

Typically λ_L = 1 μm and θ_e = 1 keV, so that we may take $x << 1$ in Eq. (4) and write

$$\lim_{x \to o} f(x) = \ell n \frac{2}{x} - .5772 = \ell n\ (2.25\ \theta_e/h\nu). \tag{6}$$

In a purely classical treatment of collisional absorption, f(x) is replaced by $\ell n\Lambda$. The present discussion would more appropriately be labelled "linear" absorption.

When the electron-ion collision frequency $\nu_{ei} << \omega$, the refractive index of the underdense plasma is simply

$$N = \sqrt{1 - \omega_p^2/\omega^2} = \sqrt{1 - n_e/n_c}, \quad \omega_p < \omega \tag{7}$$

Thus, inverse bremsstrahlung absorption is most effective for high Z materials at relatively low electron temperatures. Restricting our attention to an isothermal plasma, let us write

$$\kappa = \kappa_o(\theta_e) \frac{n_e^2}{N}. \tag{8}$$

The total absorption suffered by a ray as it passes in and out of the corona is then given by

$$\Phi_{ABS} = \Phi_{IN}\ (1 - e^{-\kappa_o A}). \tag{9}$$

The quantity $p = \kappa_o A/2$ is the optical thickness.

We shall refer to

$$A = 2 \int_0^\infty \frac{n_e^2}{N} \, d\ell \tag{10}$$

as the absorption integral.

The phase and group velocities are given by

$$v_p = \frac{c}{\sqrt{1 - \omega_p^2/\omega^2}} \tag{11}$$

$$v_G = c^2/v_p = c\sqrt{1 - \omega_p^2/\omega^2} \, , \tag{12}$$

showing clearly that the laser energy spends most of its time near the critical surface where the bulk of the absorption takes place. A relevant quantity of interest is the energy transit time (in and out):

$$t_T = 2 \int \frac{d\ell}{v_G} = \frac{2}{c} \int \frac{d\ell}{\sqrt{1 - \omega_p^2/\omega^2}} \, . \tag{13}$$

In order for ray tracing studies to make sense, t_T must be much less than the laser pulse length. Even more restrictedly, there must not be significant changes in the intensity in a time t_T. To evaluate the transit time integral (13), let us assume an exponential density profile

$$n_e = n_c e^{-x/L}, \tag{14}$$

where x is distance measured from the critical surface and L is the scale height. This profile is fairly accurate for isothermal atmospheres at relatively low laser intensities.[14] Then, at normal incidence,

$$t_T = \frac{2}{c}\int_0^X \frac{dx}{\sqrt{1 - e^{-x/L}}} \quad , \tag{15}$$

where X is chosen where the plasma density becomes negligibly tenuous. Carrying out the integral, we find

$$t_T = \frac{2X}{c} + \frac{4L}{c}\,\ell n\,(1+\sqrt{1 - e^{-X/L}}). \tag{16}$$

Let us choose X large enough that $e^{-X/L} \ll 1$. Then

$$t_T \approx \frac{2X}{c} + (4\ell n2)\,\frac{L}{c}. \tag{17}$$

Since 2X/c is just the vacuum travel time, we see that the energy lag time is simply

$$\Delta t_T \approx 4\ell n2\,\frac{L}{c} = 2.773\,\frac{L}{c}\,. \tag{18}$$

For small pellets, L ≈ 100 μm, so that $\Delta t_T \approx 0.9$ psec. If X = 300 μm, the total transit time through the plasma is about 3.0 psec, still a very short time, even for 40 psec pulses. For very steeply rising pulses there is the possibility of some pulse shape distortion by the time the laser energy reaches the critical surface, due to the time dependence of L.

Another approximation made in deriving the linear absorption coefficient is the transparency condition,

$$\nu_c/\omega_L \ll 1, \tag{19}$$

where ν_c is the electron-ion collision frequency. The full classical absorption coefficient may be written

$$\kappa = \frac{2\omega_L}{c}\left[-\frac{\beta}{2} + \frac{1}{2}\sqrt{\beta^2 + (1-\beta)^2\,(\nu_c/\omega_L)^2}\right]^{1/2}, \tag{20}$$

where

$$\beta \equiv 1 - \frac{\omega_p^2}{\omega_L^2 + \nu_c^2} \tag{21}$$

When (19) is satisfied this simplifies to

$$\kappa^{(o)} = \left(\frac{\omega_p}{\omega_L}\right)^2 \left(\frac{\nu_c}{v_G}\right) . \tag{22}$$

As a sufficient condition for transparency let us evaluate (22) at the critical surface where the absorption is strongest:

$$v_G \kappa_c^{(o)} = \nu_c << \omega_L . \tag{23}$$

Kidder shows[5] that, for $\lambda_L = 1.06$ μm,

$$v_G \kappa_c^{(o)} = \frac{3\ \ell n\Lambda\ cZ_{eff}}{\theta_e^{3/2}}\ cm^{-1}, \tag{24}$$

with θ_e in KeV. Using (24) in (23) then gives the result,

$$\frac{Z_{eff}\ \ell n\Lambda}{\theta_e^{3/2}} << 2 \times 10^4 \tag{25}$$

Since $\ell n\Lambda$ lies in the range 5-10 for kilovolt temperatures, we see that the transparency condition is well met for DT or glass, but might be violated for higher Z materials.

The classical absorption coefficient (2) is subject to several restrictions. First of all, at normal incidence, when the ray penetrates to the critical surface, the geometrical optics approximation breaks down. Dawson, Kaw and Green[15] show that consideration of the full wave equation gives an increase in absorption over that predicted by (2).

A veritable host of pronounced nonlinear effects come into play at higher laser intensities, perhaps the most important being density profile modification due to ponderamotive forces,[16] and resonance absorption[1]. Other effects include self-focusing in the plasma itself,[16] stimulated Brillouin and Raman scattering,[12] and parametric instabilities.[16] For reactors, one might consider 1 MJ of 5000 Å laser radiation with a peak power of 1000 TW incident on pure DT shells of radius 1 mm. These parameters imply intensities of about 10^{16} W/cm^2 and electron temperatures in the 10 KeV range. Thus, relatively small collisional absorption in highly non-isothermal atmospheres, strong density steepening, and (hopefully) enhanced resonance absorption can be expected.

With these caveats, let us as a first step evaluate the absorption integral (10) under the very simplified conditions of an isothermal exponential density profile.

3. Absorption at Oblique Incidence

In a previous report[10] we found that at least 12 and probably 20 beams would be required to yield acceptably uniform irradiance over the pellet surface. However, a price must be paid for such high uniformity in the form of non-normal incidence and consequent refractive losses. The primary aim of this section is to estimate the magnitude of these losses in a conceptual laser fusion reactor.

Generally we find that for physically realistic spatial beam profiles, the integrated absorption does not depend strongly on the maximum angle of incidence, due to the concentration of beam power near the optical axis. However, the weighted average ("effective") angle of incidence usually turns out to exceed the range where resonance absorption is expected to be strongest. It should be emphasized that the present work takes no account of such non-linear effects as self-steepening[16] of the density profile, due to the substantial ponderamotive forces generated at high laser intensities.

3.1 Slab Geometry

Consider a ray incident at angle Ψ on an infinite isothermal slab of plasma, as illustrated in Figure 2. Assuming the density profile[17]

$$n_e = \begin{cases} n_c e^{-x/L} & x < X \\ 0 & x > X \end{cases} \qquad (26)$$

we can find the ray path in the x-y plane as follows. From the invariant

$$N(x)\,\sin\theta = \sin\Psi\ , \tag{27}$$

where θ is the angle between the normal and the local tangent, we find

$$N(x_{min}) = \sin\Psi \tag{28}$$

$$y_{min} = \sin\Psi \int_{x_m}^{X} \frac{dx}{\sqrt{N^2 - \sin^2\Psi}}\ . \tag{29}$$

Since

$$N = \sqrt{1 - e^{-x/L}} \tag{30}$$

we have

$$x_{min} = 2L\ \ell n\ \sec\Psi \tag{31}$$

and

$$y_{min} = X\tan\Psi + 2L\tan\Psi\ \ell n\ (\cos\Psi + \sqrt{\cos^2\Psi - e^{-X/L}}\ )\ . \tag{32}$$

A quantity useful for computing the uniformity of energy deposited near the critical surface is the <u>net displacement</u>

$$\Delta y = y_{min} - X\tan\Psi \tag{33}$$

or

$$\Delta y = 2L\tan\Psi\ \ell n\ (\cos\Psi + \sqrt{\cos^2\Psi - e^{-X/L}}\ )\ . \tag{34}$$

When Ψ is small, this reduces to

$$\Delta y \approx 2L\ \Psi\ \ell n\ (1 + \sqrt{1 - e^{-X/L}}\ )\ , \tag{35}$$

and when $X >> L$, Eq. (34) becomes

$$\Delta y \approx 2L\tan\Psi\ \ell n\ (2\cos\Psi)\ . \tag{36}$$

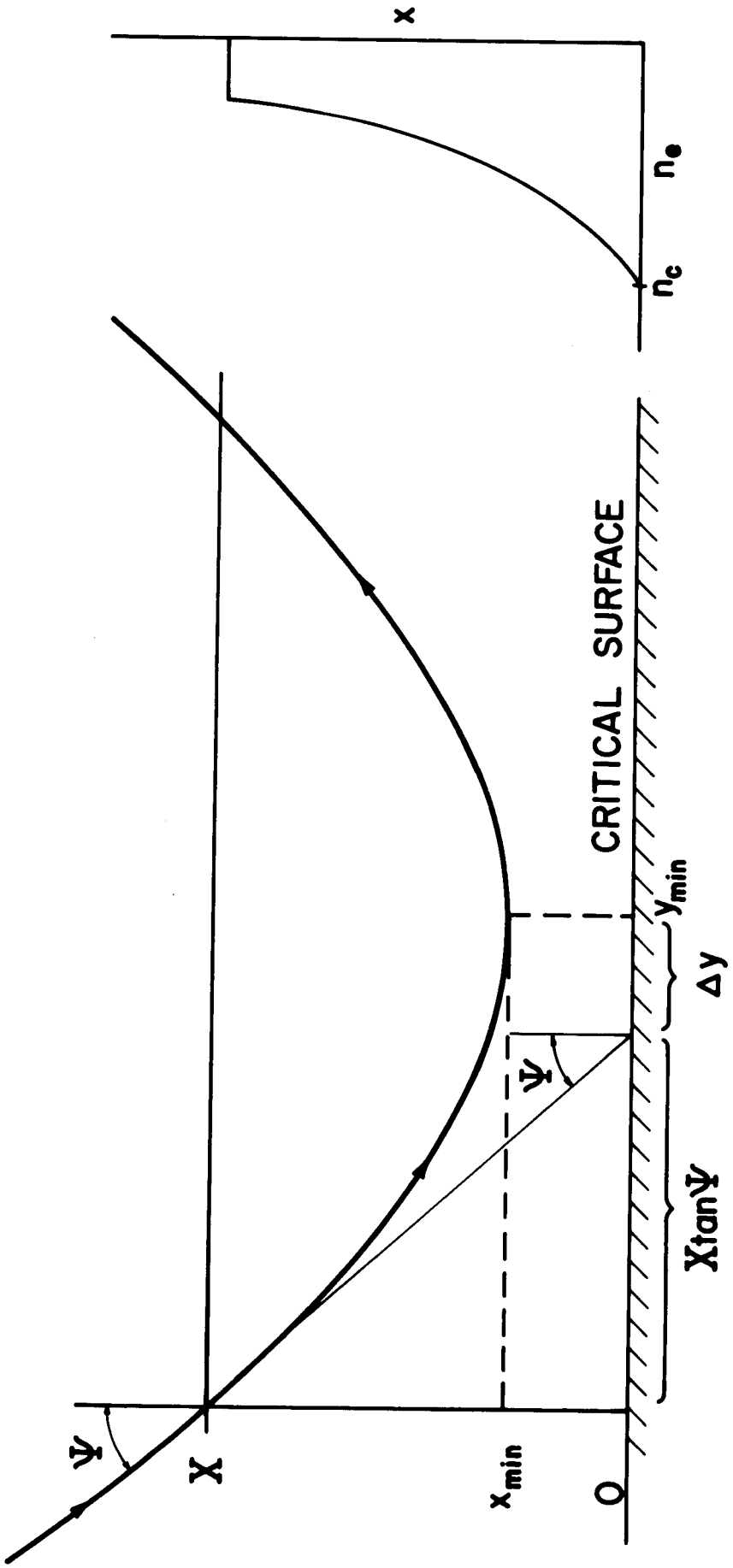

FIGURE 2

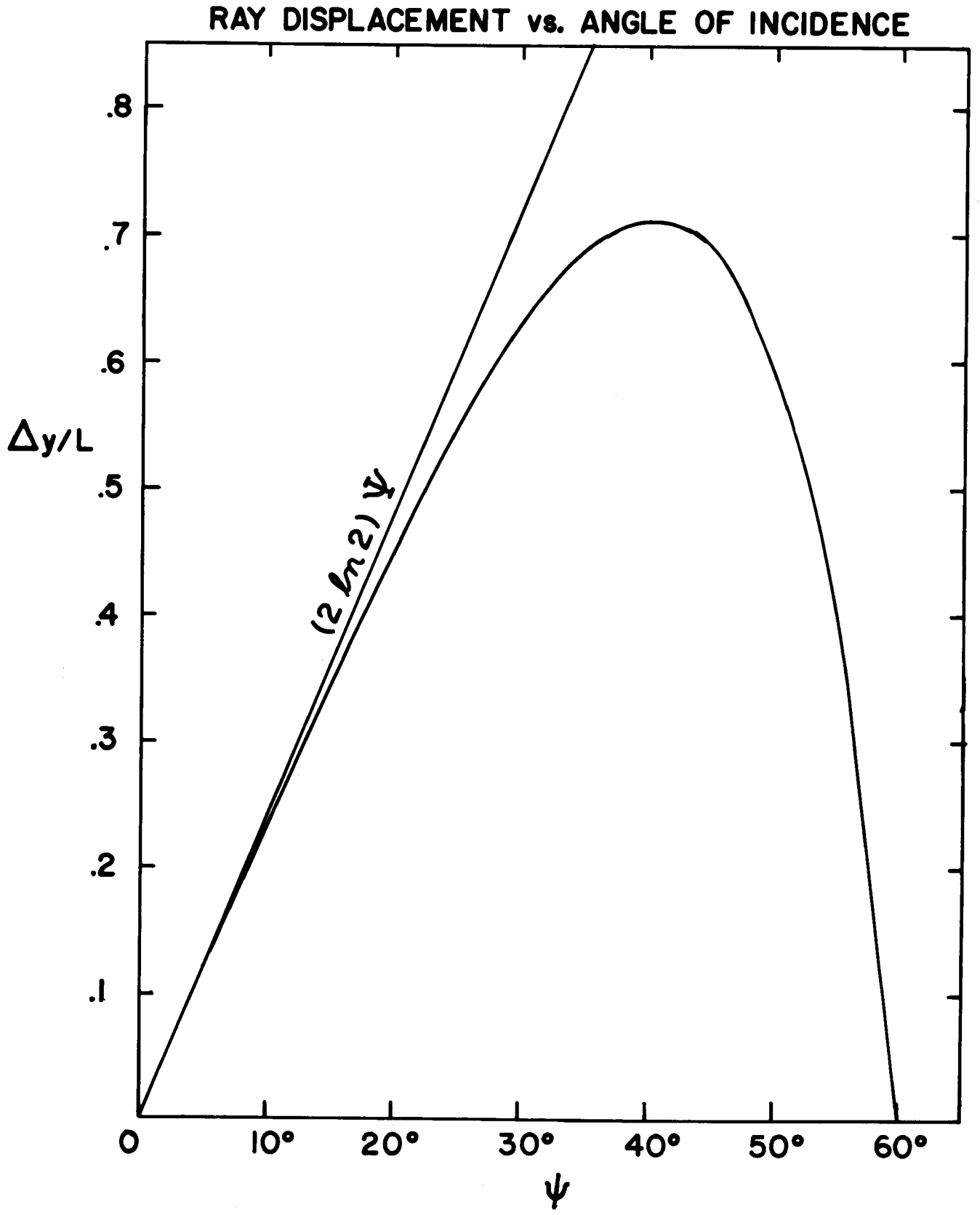
RAY DISPLACEMENT vs. ANGLE OF INCIDENCE
Δy/L
.8
.7
.6
.5
.4
.3
.2
.1
(2 ln 2) Ψ
0
10°
20°
30°
40°
50°
60°
Ψ

FIGURE 3

Note that Δy reaches a maximum for some value of Ψ, as Fig. 3 shows for the case $X >> L$.

The absorption integral (10) becomes

$$A = 2 \int_{x_m}^{X} \frac{n_e^2}{N} \frac{d\ell}{dx} dx = 2 \int_{x_m}^{X} \frac{n_e^2 \, dx}{\sqrt{1 - n_e/n_c} \cos\theta} \quad . \tag{37}$$

For the exponential profile (26), this may be written

$$A = 4L \int_{\sin\Psi}^{N_1} \frac{N (1 - N^2) \, dN}{\sqrt{N^2 - \sin^2\Psi}} \quad , \tag{38}$$

where $N_1^2 = 1 - e^{-X/L}$. Thus,

$$A = \frac{8L}{3} \sqrt{\cos^2\Psi - e^{-X/L}} \; (\cos^2\Psi + \frac{1}{2} e^{-X/L}) \quad . \tag{39}$$

When $X >> L$,

$$A = \frac{8L}{3} \cos^3\Psi \quad . \tag{40}$$

This formula is widely used in estimating the effect of oblique incidence on absorption. In the next section, we shall derive the analogue in spherical geometry as an asymptotic series in L. A case of interest is $\Psi << 1$, but $e^{-X/L}$ not small. We find

$$A = \frac{8L}{3} (1 + \frac{1}{2}\gamma) \sqrt{1 - \gamma} \left[1 - \frac{3 (2 - \gamma)}{2 (1 - \gamma) (2 + \gamma)} \Psi^2\right] , \tag{41}$$

where $\gamma \equiv e^{-X/L}$. Equations (36) and (40) have been previously derived by Brueckner.[18] Shearer[19] obtains a $\cos^5\Psi$ law for linear density profiles.

3.2 Spherical Geometry

Figure 1 shows a ray impinging on a spherically symmetric isothermal plasma. Note that in this case the projected angle of incidence at

r_{crit}, Ψ, differs from the exterior angle Ψ_o. When N = N(r), an invariant exists, known as Bouger's Law,[20]

$$rN(r)\sin\theta = r_c \sin\Psi = r_m N(r_m) = R\sin\Psi_o. \tag{42}$$

For small Ψ, (42) yields

$$r_{min} \approx r_c + \frac{n_c}{|n_c'|}\sin^2\Psi . \tag{43}$$

For larger Ψ, this is a good starting point for an iterative solution of (42). For an exponential density profile,

$$r_m \approx r_c + L\sin^2\Psi . \tag{44}$$

While the angular displacement θ_{min} is readily calculated, we shall omit it here, since for multibeam systems, uniformity is of interest only at early times, when the scale height is short enough for the slab result (34) to apply. The absorption is

$$A = 2\int_{r_m}^{\infty} \frac{n_e^2}{N}\frac{d\ell}{dr}\,dr , \tag{45}$$

where we have taken $r \to \infty$ for simplicity. From Fig. 1

$$d\ell = dr\sec\theta . \tag{46}$$

Thus,

$$A(\Psi,L) = 2\int_{r_m}^{\infty} \frac{rn_e^2 dr}{\sqrt{r^2N^2 - \sin^2\Psi}} , \tag{47}$$

where r_c has been scaled out. Note that A depends on Ψ and L through the lower limit of integration as well as the integrand itself. Numerical evaluation of (47) is complicated by the singularity at r_m, even though N(r) doesn't vanish for $\Psi \neq 0$. At normal incidence, (47) reduces to

$$A_\perp = 2 \int_{r_c}^{\infty} \frac{n_e^2 \, dr}{\sqrt{1 - n_e/n_c}} \quad . \tag{48}$$

On this case the integrand is singular at r_c because N = 0. For the exponential density profile we again obtain

$$A_\perp = \frac{8L}{3} \quad . \tag{49}$$

At oblique incidence, closed form expressions for A do not seem to exist. However, two limiting cases may be treated analytically; (a) small incident angles, for arbitrary L; and (b) small L, for which the slab geometry results apply.

Before proceeding to these special cases, let us ask whether L can be predicted <u>a priori</u>. In slab geometry, the "isothermal blowoff model" gives[17]

$$L = v_s t \tag{50}$$

where

$$v_s = \left(\frac{n_i \theta_i + n_e \theta_e}{m_i} \right)^{1/2} \approx \left(\frac{n_e \theta_e}{m_i} \right)^{1/2} \tag{51}$$

is the isothermal sound speed.

In spherical geometry, numerical studies and experiments suggest that a better model may be

$$n_e = n_c \left(\frac{r_c}{r} \right)^2 e^{-(r - r_c)/L} \quad . \tag{52}$$

The effective scale height at r_c is therefore

$$L_{true} = -\frac{n_c}{n_c'} = \frac{L}{1 + 2L/r_c} \quad . \tag{53}$$

At early times the slab result is recovered, but at later times,

$$L_{true} \to r_c/2 \quad . \tag{54}$$

In most cases of interest we may let $R \to \infty$ in the absorption integrals, the expansion front typically extending to about three scale heights or so. Figure 4 shows the normalized absorption integral $A/A_\perp$ as a function of Ψ for various scale heights for the exponential density profile (26). As one would expect, the slab result,

$$A/A_\perp = \cos^3\Psi \tag{55}$$

is recovered as $L \to 0$. In fact, because the curves cross near $\Psi = 30^0$, eq. (55) fits to within 5% for $L < 1$, $\Psi \leq 30^0$. Thus, curvature <u>decreases</u> absorption slightly at small angles of incidence, but substantially <u>increases</u> absorption at larger Ψ due to the increased path length in the plasma.

An asymptotic expansion of $A(\Psi,L)$ for $\Psi << 1$ may be carried out as follows. Taking

$$z^2 = N^2 - \frac{\sin^2\Psi}{r^2} \tag{56}$$

eq. (47) may be manipulated into the (exact) form

$$A/A_\perp = 1 - \frac{3}{2}(I_1 + I_2)\sin^2\Psi, \tag{57}$$

where

$$I_1 = \int_0^1 \frac{dz}{r^2} \tag{58}$$

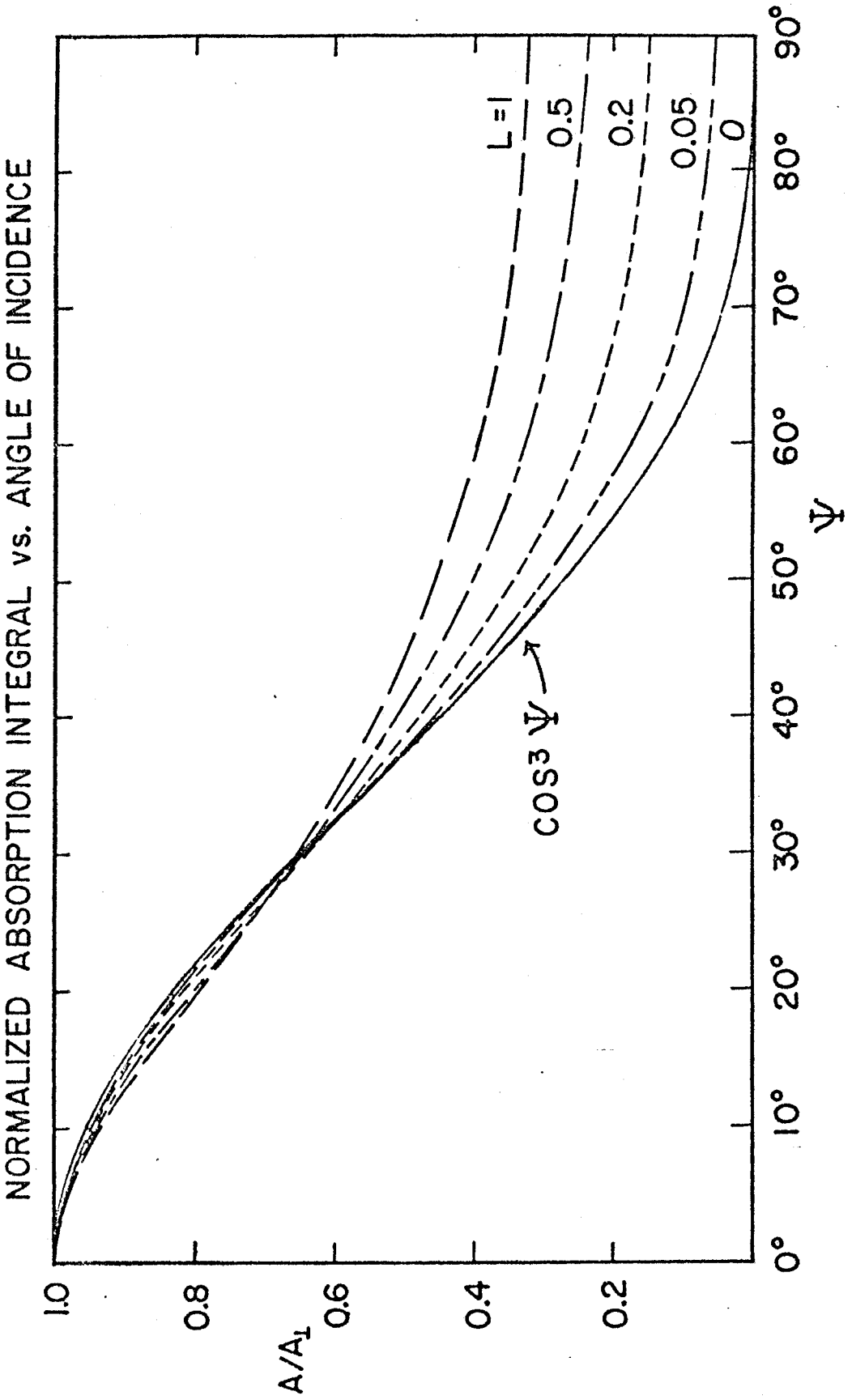
NORMALIZED ABSORPTION INTEGRAL vs. ANGLE OF INCIDENCE
A/A1
1.0
0.8
0.6
0.4
0.2
0°
10°
20°
30°
40°
50°
60°
70°
80°
90°
Ψ
L=1
0.5
0.2
0.05
0
COS3 Ψ

FIGURE 4

$$I_2 = \int_{r_m}^{\infty} \frac{e^{-x/L}}{r^3 z}\, dr \ , \tag{59}$$

where $x = r-1$, all distances being measured in units of r_c. For small Ψ,

$$I_1' = \tilde{I}_1 + I_1' \sin^2\psi \tag{60}$$

$$I_2 = \tilde{I}_2 + I_2' \sin^2\psi, \tag{61}$$

where

$$\tilde{I}_1 = 2\int_0^{\infty} \frac{\sqrt{1 - e^{-x/L}}}{(1+x)^3}\, dx \sim 1 - 1.227L + 6.522L^2 - \ldots \tag{62}$$

$$\tilde{I}_2 = 6L\int_0^{\infty} \frac{\sqrt{1 - e^{-x/L}}}{(1+x)^4}\, dx \sim 2L - 3.681L^2 + 13.04L^3 - \ldots \tag{63}$$

and

$$I_1' = -\int_0^{\infty} \frac{dx}{(1+x)^5 \sqrt{1 - e^{-x/L}}} \tag{64}$$

$$I_2' = -5L\int_0^{\infty} \frac{dx}{(1+x)^6 \sqrt{1 - e^{-x/L}}} \tag{65}$$

This gives the desired expansion

$$A/A_{\perp} \sim 1 - \frac{3}{2}(\tilde{I}_1 + \tilde{I}_2)\sin^2\psi + \frac{3}{2}(I_1' + I_2')\sin^4\psi \ , \tag{66}$$

from which

$$\lim_{\psi \to 0} A/A_{\perp} = 1 - \frac{3}{2}(\tilde{I}_1 + \tilde{I}_2)\psi^2 \ . \tag{67}$$

This formula is very accurate for $L \leq 1$ and $\Psi < 10^{\circ}$. From the asymptotic expansions (62) and (63) we see

$$\lim_{\substack{\Psi \to 0 \\ L \to 0}} A/A_{\perp} = 1 - \frac{3}{2}\Psi^2 (1 + 0.773\, L) \quad . \tag{68}$$

in agreement with the slab result as $L \to 0$ and accurate to 0.1% for $L < .2$, $\Psi < 10^{o}$.

In general, our attempts to improve on the $\cos^3\Psi$ approximation to $A/A_{\perp}$ were disappointing, only modest improvements resulting for $L < 0.2$, $\Psi < 40^{o}$ or for $L < 1.0$, $\Psi < 10^{o}$.

4. Total Power Absorbed at Oblique Incidence

In estimating the total laser power absorbed by a pellet we must take into account the distribution of angles of incident due to

(1) The specific optical element (lens or mirror) employed

(2) The spatial beam profile incident on that element

Consider then an annular flux tube incident on a spherical target whose center is located a distance Δx inside the focus f, as depicted in Fig. 5 (assuming lenses for concreteness). The plasma corona is assumed to extend to an outer radius R, outside of which negligible absorption and refraction occur. The projected angle of incidence Ψ and lens angle ξ are related by

$$\sin\Psi = \frac{\Delta x}{r_c} \sin\xi \quad , \tag{69}$$

where

$$\tan\xi = \frac{r_L}{f} \tag{70}$$

Recall that the f/no. is

$$F = f/2R_L \quad . \tag{71}$$

In eq. (69) we assume that the critical radius remains near the original pellet radius, so that Ψ is a known function of the lens radius r_L. In reality r_c usually expands by about 50%, which enhances absorption, as will be seen in the next section.

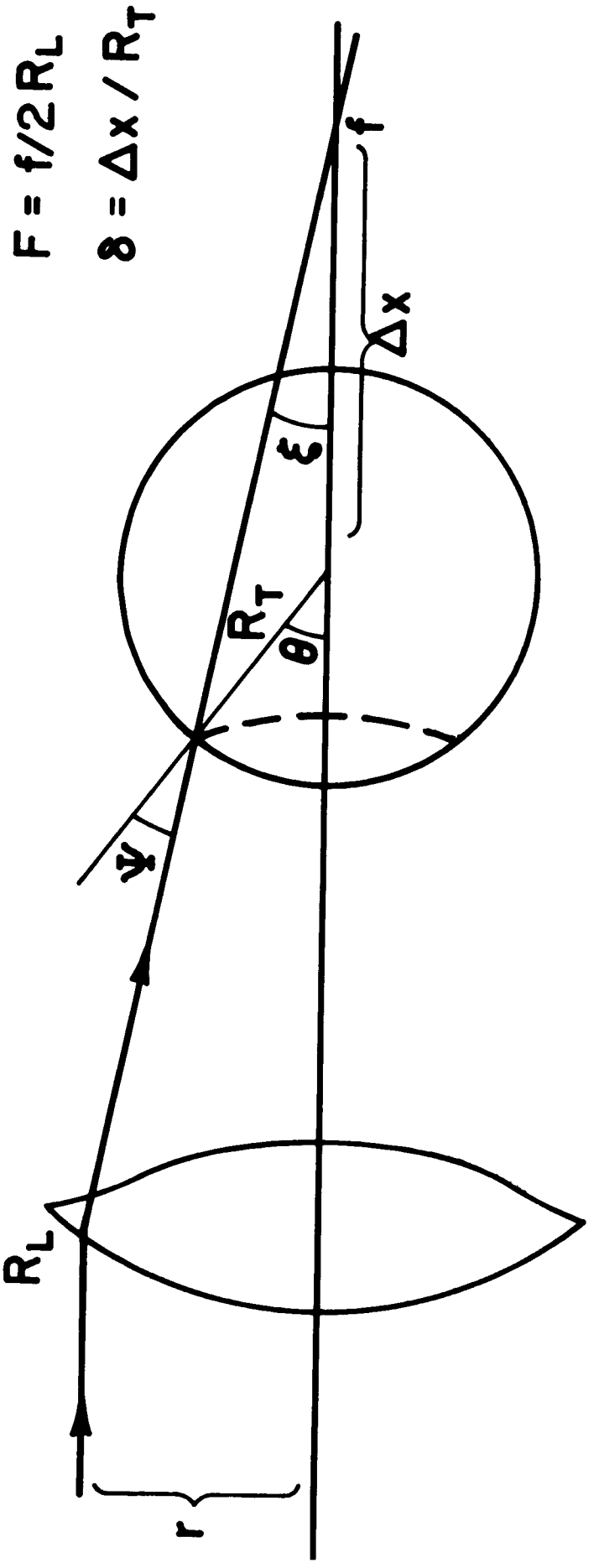

FIGURE 5

The flux Φ_{in} (w/cm^2) incident on the pellet at $r = R$ is related to the flux on the lens $\Phi_L(r_L)$ by

$$\Phi_L \, dA_L = \Phi_{in} \, dA_{in} \, , \tag{72}$$

which yields an expression for the target irradiance

$$\Phi_{in} = \Phi_L(r_L) \left(\frac{f}{R}\right)^2 \frac{1 + \frac{\Delta x}{R} \cos\theta}{(\cos\theta + \frac{\Delta x}{R})^3} \, . \tag{73}$$

To calculate the total absorption, we first observe that in the presence of focusing, the exponential law, eq. (1) must be replaced by

$$\frac{\partial \Phi}{\partial \ell} = -\kappa\Phi + \left(\frac{\partial \Phi}{\partial \ell}\right)_{foc} \, . \tag{74}$$

An infinitesimal flux tube of cross sectional area δa encloses a power

$$\delta P = \Phi \delta a. \tag{75}$$

Along this flux tube,

$$\left(\frac{\partial \Phi}{\partial \ell}\right)_{foc} = - \frac{\Phi}{\delta a} \frac{\partial}{\partial \ell} \delta a. \tag{76}$$

Using this expression in eq. (74) and integrating then yields

$$\delta P_{out} = \delta P_{in} e^{-\int_0^{\ell} \kappa d\ell} \, . \tag{77}$$

Thus, it is <u>power</u>, not flux, that obeys an exponential absorption law.

To apply eq. (77) to the problem at hand, let us integrate over all flux tubes incident on the pellet

$$P_{out} = \int e^{-\int \kappa d\ell} \, dP_{in} = \int e^{-\int \kappa d\ell} \, dP_L. \tag{78}$$

The total power incident on the lens is

$$P_{in} = P_L = \int \Phi_L(r_L) dA_L. \tag{79}$$

The fractional absorption is therefore

$$n_{AB} = 1 - \frac{P_{out}}{P_L} = 1 - \frac{\int_0^{R_L} \Phi_L \, e^{-\kappa_o A_\perp \cos^3 \Psi} \, r_L dr_L}{\int_0^{R_L} \Phi_L r_L dr_L} \, , \tag{80}$$

where $\Psi(r)$ is given by (69) and (70). Finally we may define an "effective angle of incidence" by

$$P_{out} = P_L \, e^{-\kappa_0 A_\perp \cos^3\Psi_{eff}} \quad . \tag{81}$$

As a specific example let us take

$$\Phi_L(r_L) = \Phi_0 \, e^{-(r_L/a)^3} \quad , \tag{82}$$

with a = 0.70. This beam profile, depicted in Fig. 6, gives good uniformity[10] for 20 f/1.5 lenses and a beam overlap $\theta_{max} \gtrsim 50°$. To complete the necessary algebra we have, from Fig. 5,

$$\delta = \Delta x/r_c = 2F \sin\theta_{max} - \cos\theta_{max} \tag{83}$$

$$\sin\theta_{max} = \frac{2F\delta + \sqrt{1 + 4F^2 - \delta^2}}{1 + 4F^2} \quad . \tag{84}$$

The integrated absorption and Ψ_{eff} are shown in Figures 7 and 8 for several values of $\kappa_0 L$, with L in cm and, for $\lambda_L = 1.06$ μm,

$$\kappa_0 = \frac{3 \, \ell n\Lambda \, Z_{eff}}{\theta_e^{3/2}} \ cm^{-1} \quad .$$

Thus, if $\theta_e = 1$ keV and $Z_{eff} = 1$, $L \simeq 10^{-2}$ cm, $\kappa_0 L = .25$ and $\eta_{ab} \simeq 45\%$. η_{ab} reaches a maximum and Ψ_{eff} vanishes at $\theta_{max} = \xi = 18.4^o$, as they should. Due to the concentration of energy near the beam axis, the refractive loss at oblique incidence is quite moderate, amounting to only a few percent at $\theta_{max} = 50^o$.

For reference, Fig. 8 also shows the maximum angle of incidence, assuming f/1.5 lenses. Thus, at $\theta_{max} = 50^o$ most of the beam energy is

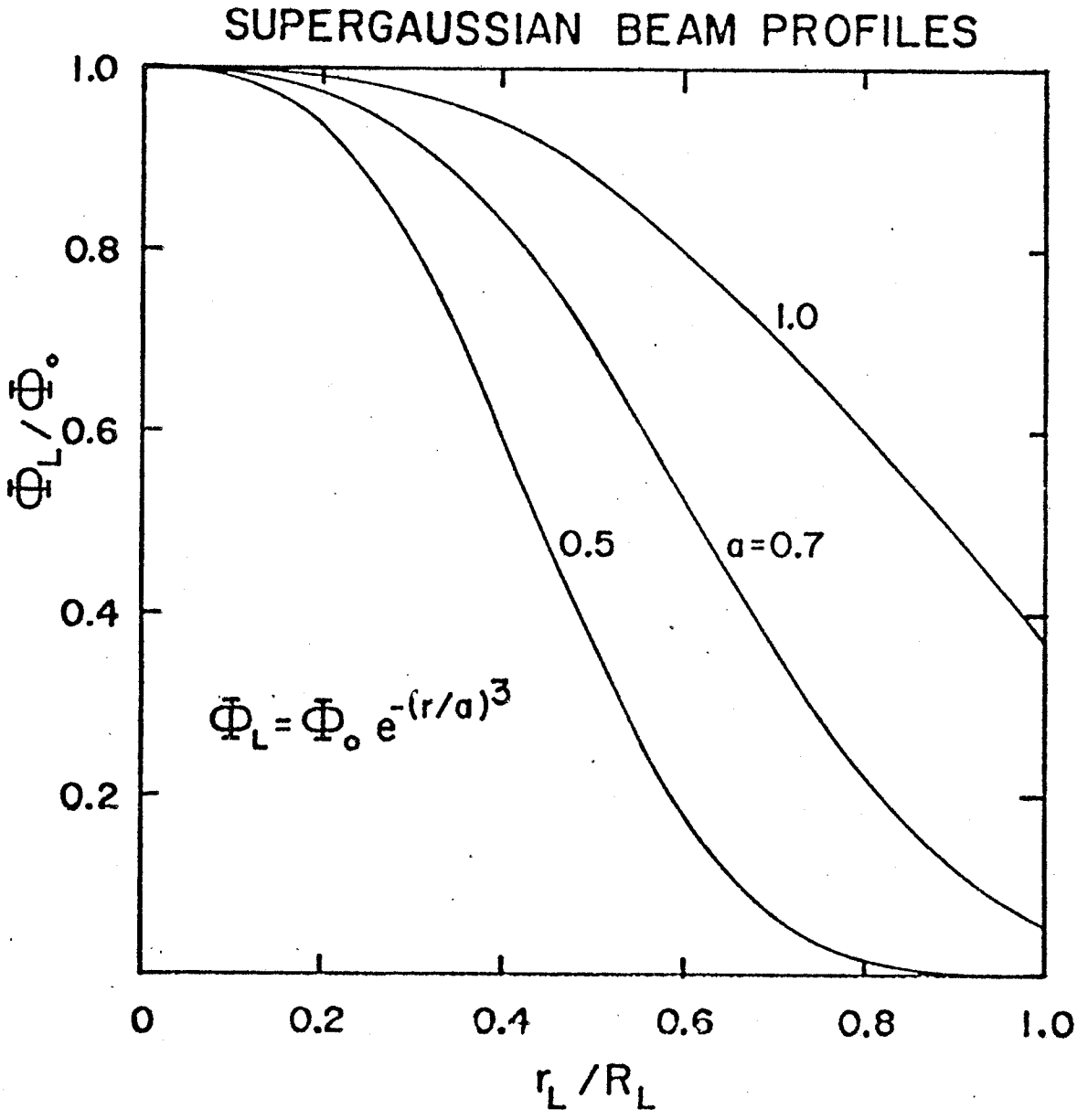
SUPERGAUSSIAN BEAM PROFILES
1.0
0.8
0.6
0.4
0.2
0
0.2
0.4
0.6
0.8
1.0
Φ_L / Φ_o
r_L / R_L
1.0
a=0.7
0.5
$\Phi_L = \Phi_o e^{-(r/a)^3}$

FIGURE 6

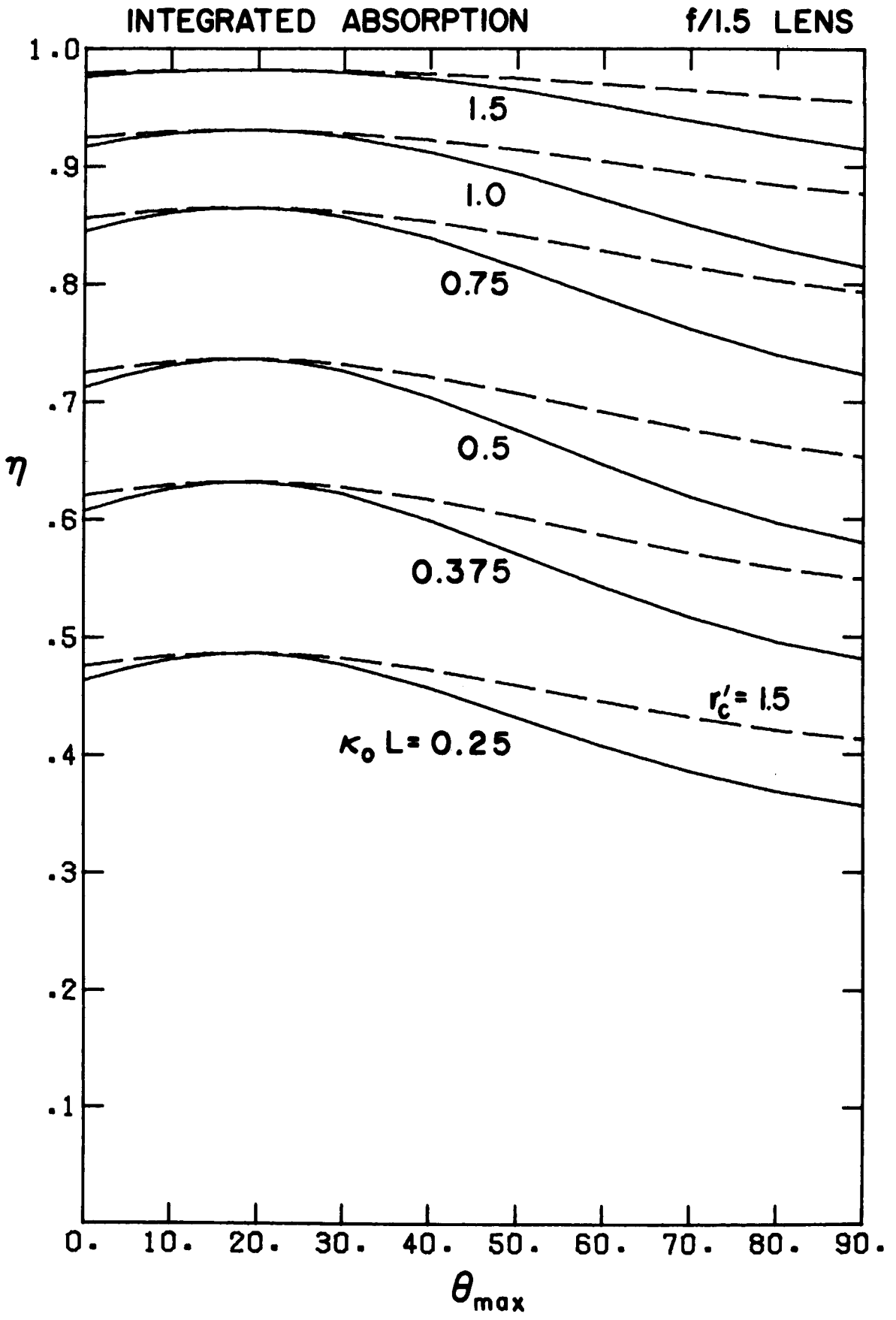
INTEGRATED ABSORPTION
f/1.5 LENS
1.0
.9
.8
.7
.6
.5
.4
.3
.2
.1
η
1.5
1.0
0.75
0.5
0.375
$r_c' = 1.5$
$\kappa_0 L = 0.25$
0.
10.
20.
30.
40.
50.
60.
70.
80.
90.
θ_{max}

FIGURE 7

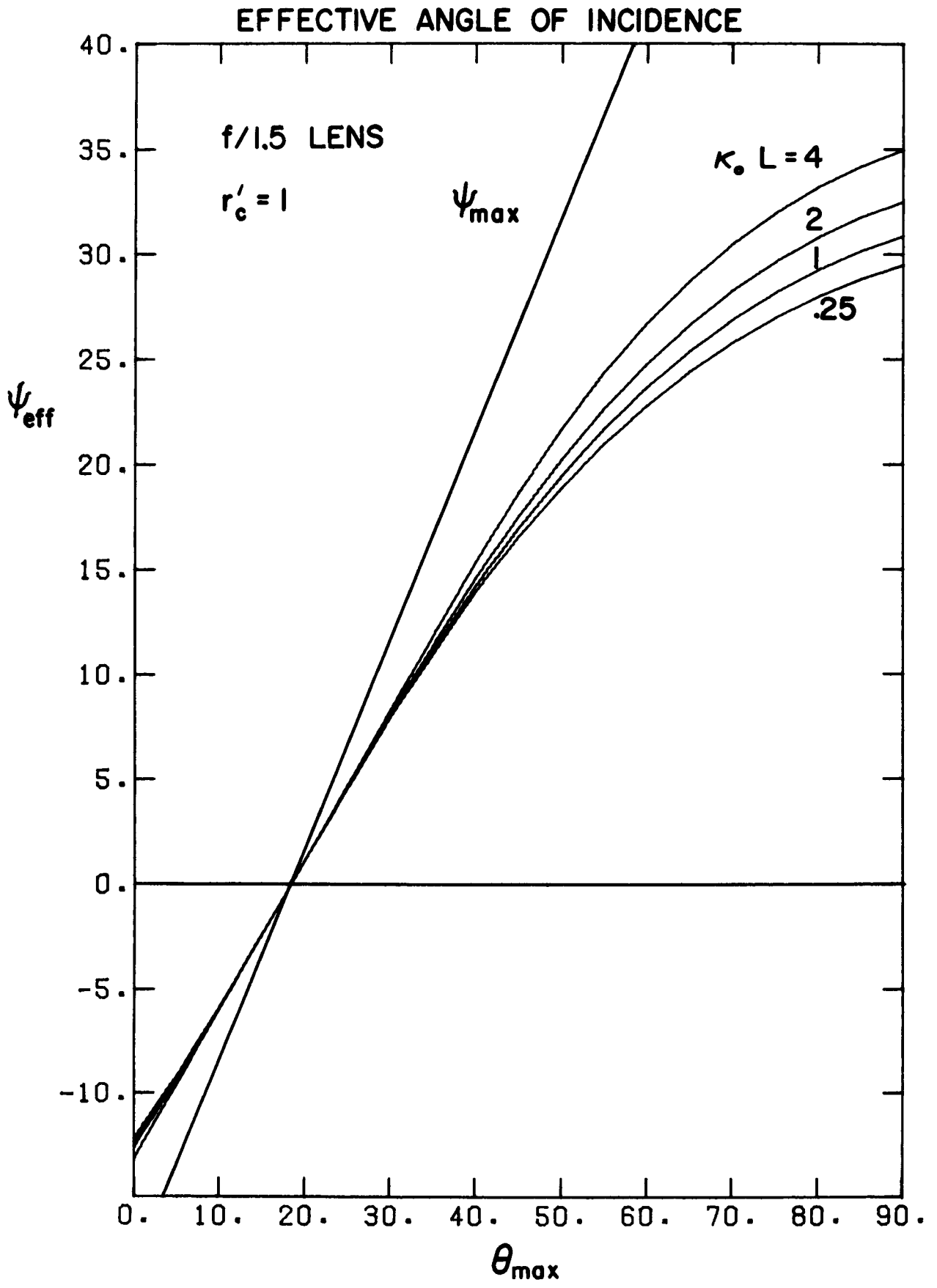
EFFECTIVE ANGLE OF INCIDENCE
f/1.5 LENS
$r_c' = 1$
ψ_{max}
$\kappa_o L = 4$
2
1
.25
ψ_{eff}
40.
35.
30.
25.
20.
15.
10.
5.
0.
-5.
-10.
0.
10.
20.
30.
40.
50.
60.
70.
80.
90.
θ_{max}

FIGURE 8

incident near $\Psi_{eff} \simeq 20^o$, considerably less than $\Psi_{max} = 31.5^o$, but still above the range for effective resonant absorption.

5. Effect of Expanding Critical Radius

When r_c increases in time, the projected angle of incidence Ψ decreases, enhancing absorption. Suppose that r_c has moved out to a position r_c'; then, as Fig. 9 shows, the angle of incidence is reduced to

$$\sin\Psi' = \frac{r_c}{r_c'} \sin\Psi \ . \tag{85}$$

Thus

$$\sin\Psi'(r_L) = \frac{r_L \left(\frac{r_c}{r_c'}\right) \delta}{\sqrt{r_L^2 + 4F^2}} \ . \tag{86}$$

Using (86) in (80) and (81) we readily define a new absorption η_{ab}' and effective angle of incidence Ψ_{eff}'.

Since $\theta' < \theta$, the effective spot size is also reduced as r_c increases. The resulting degraded uniformity of illumination is of no consequence at later times, where a substantial hot corona has been established. While it is straightforward to calculate θ'_{max}, we shall plot η_{ab}' and Ψ_{eff}' vs. θ_{max}, as this is our reference value. The integrated absorption is shown as the dashed curves in Fig. 7 for $r_c' = 1.5\ r_c$ and in Fig. 10 for $r_c' = 2.0\ r_c$. Clearly, the effect of these (quite typical) expansions is to reduce refractive losses due to nonnormal illumination to entirely negligible levels. The burden then falls on resonant absorption to absorb the remaining energy. As Figs. 11 and 12 show, the expansion

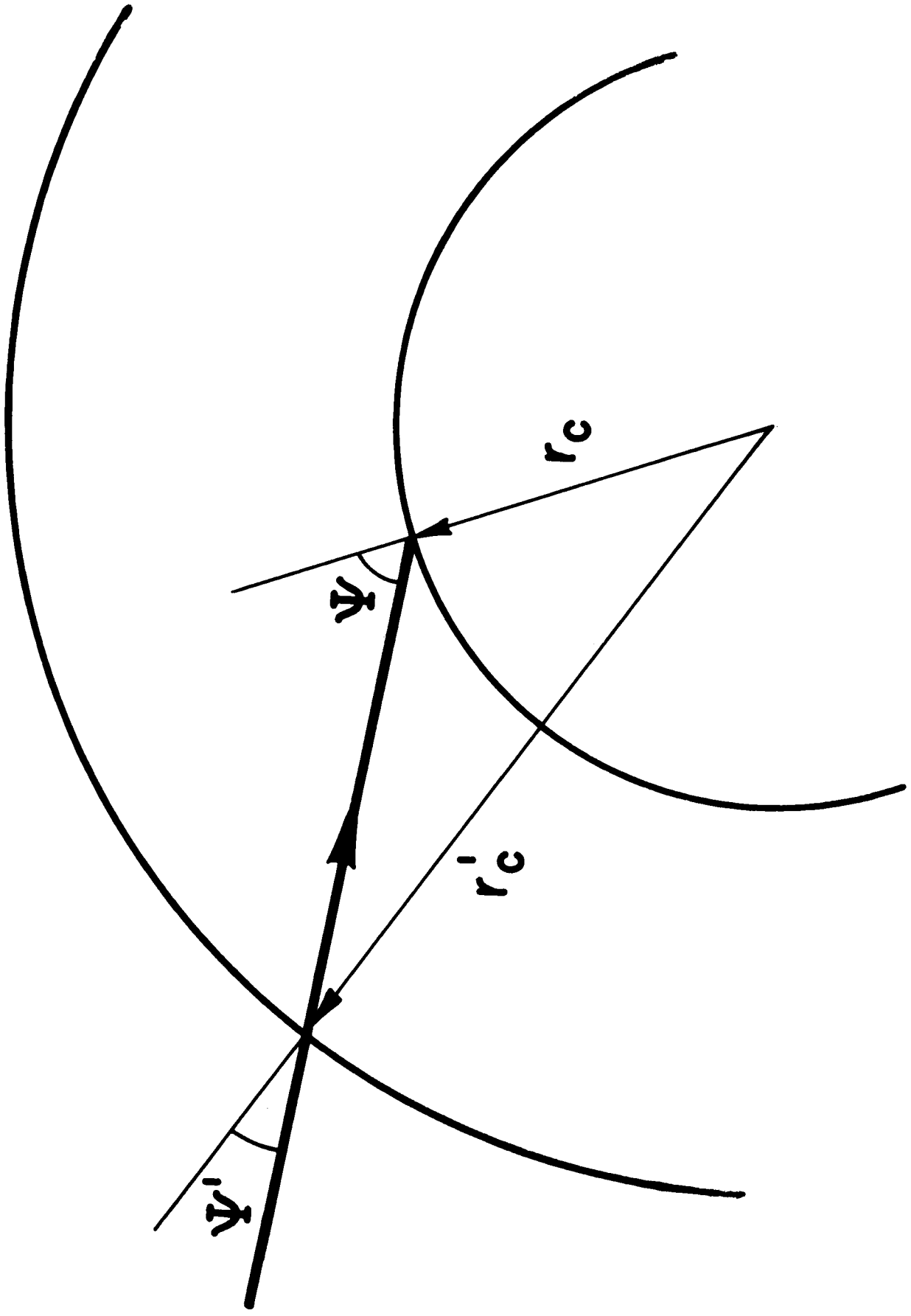

FIGURE 9

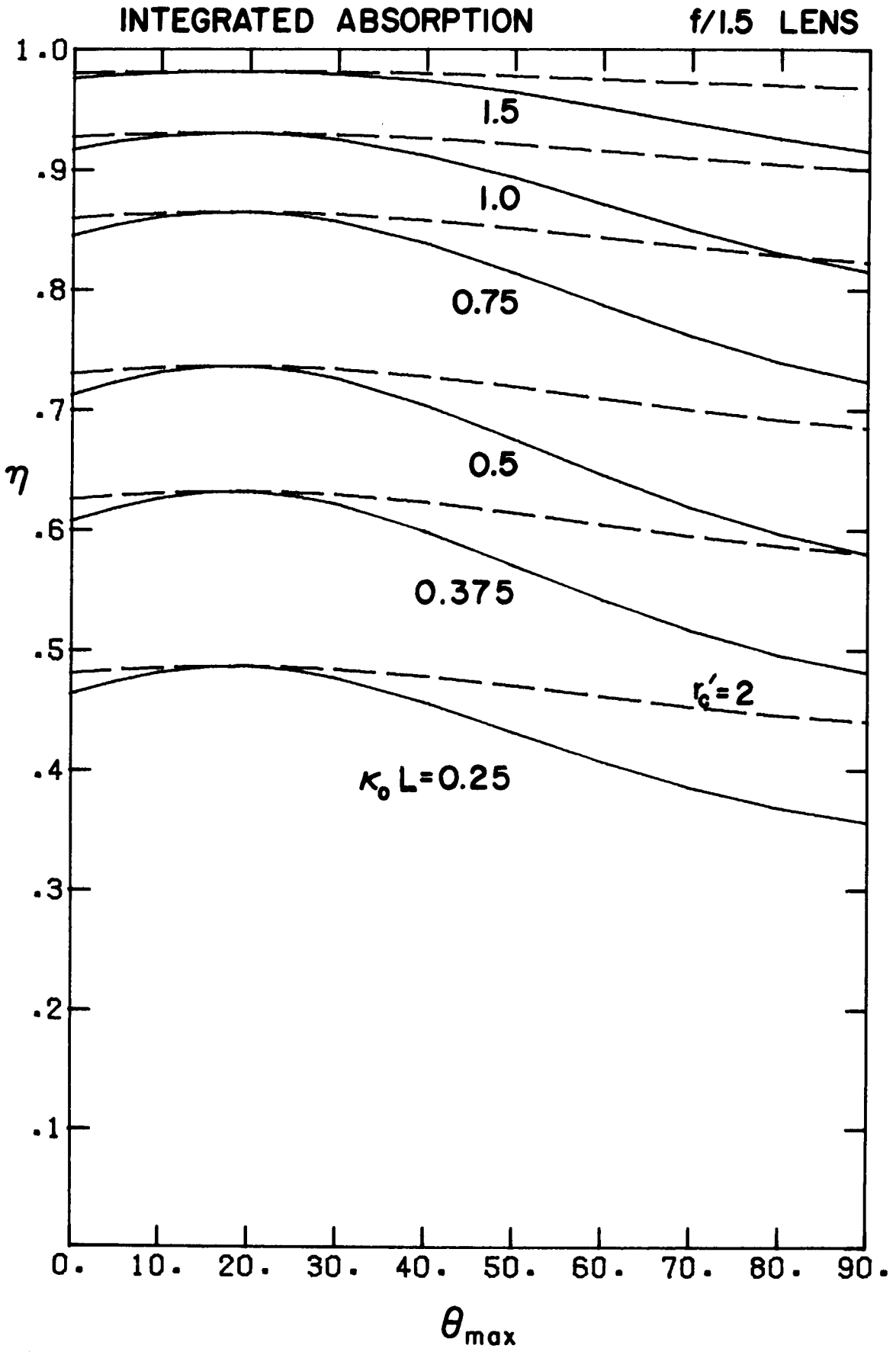
INTEGRATED ABSORPTION
f/1.5 LENS
1.0
.9
.8
.7
.6
.5
.4
.3
.2
.1
η
1.5
1.0
0.75
0.5
0.375
$r_c' = 2$
$\kappa_0 L = 0.25$
0.
10.
20.
30.
40.
50.
60.
70.
80.
90.
θ_{max}

FIGURE 10

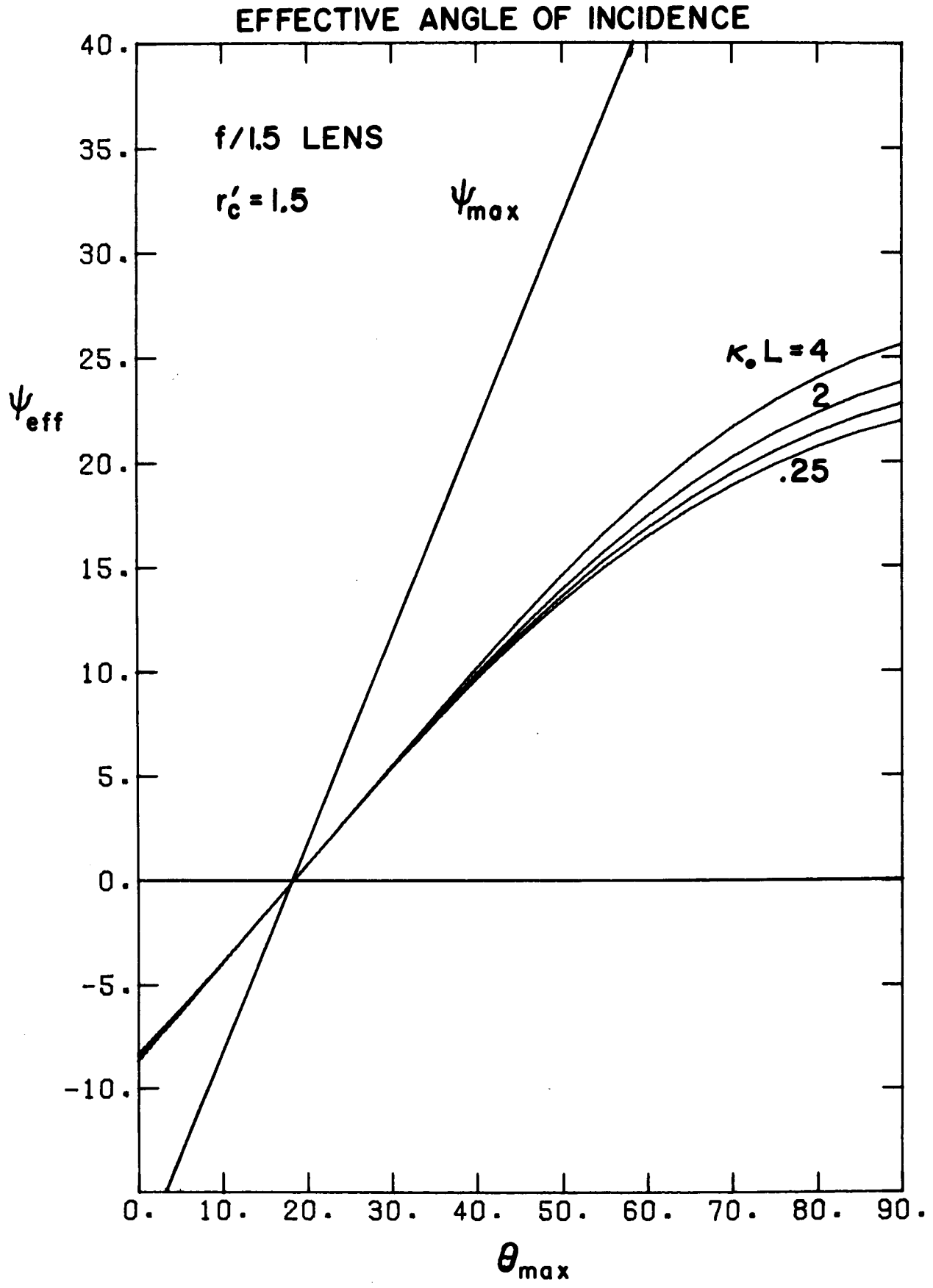
EFFECTIVE ANGLE OF INCIDENCE
f/1.5 LENS
$r_c' = 1.5$
ψ_{max}
$\kappa_o L = 4$
2
.25
ψ_{eff}
θ_{max}
40.
35.
30.
25.
20.
15.
10.
5.
0.
-5.
-10.
0.
10.
20.
30.
40.
50.
60.
70.
80.
90.

FIGURE 11

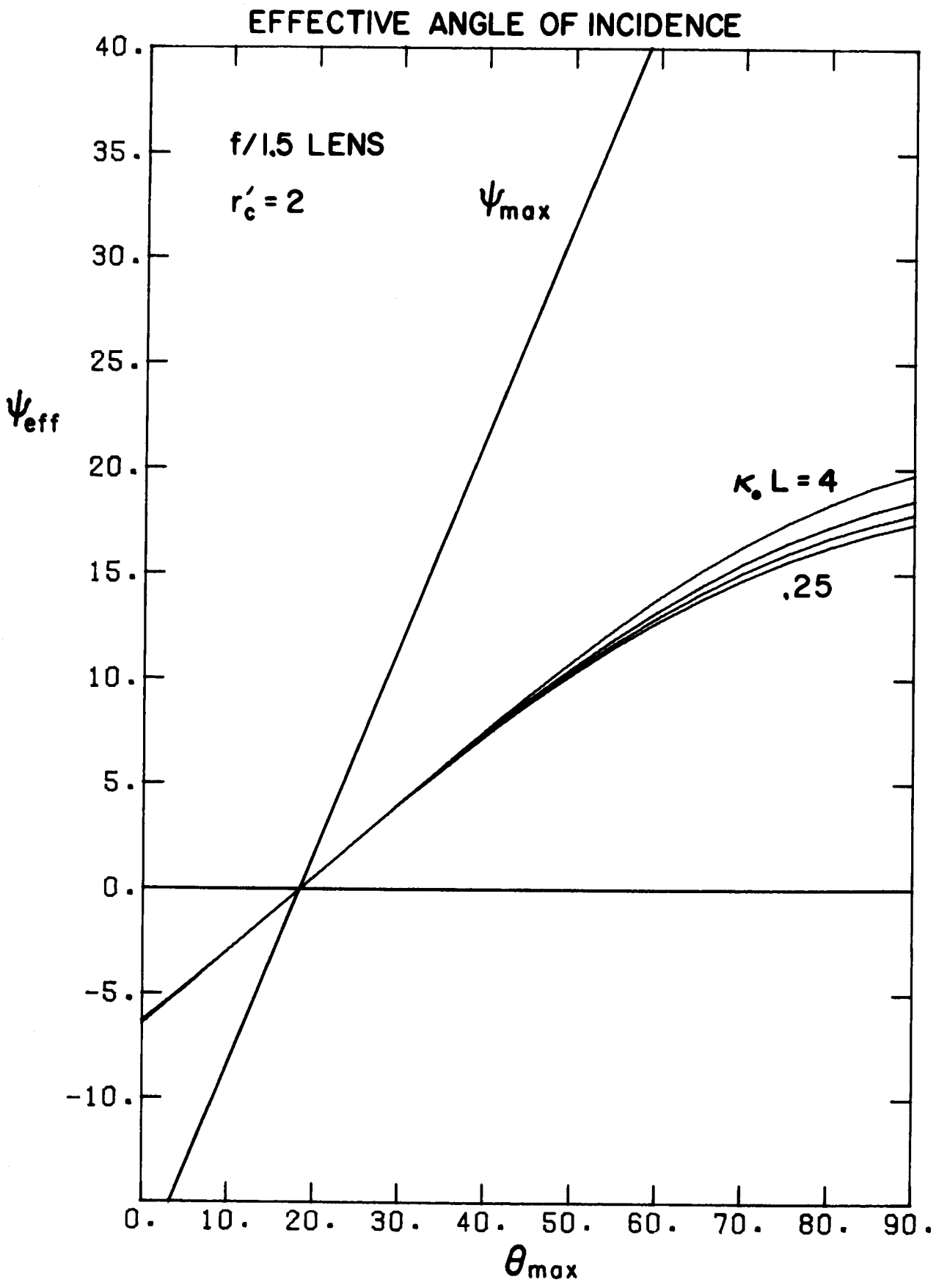
EFFECTIVE ANGLE OF INCIDENCE
f/1.5 LENS
$r_c' = 2$
ψ_{max}
$\kappa_o L = 4$
.25
ψ_{eff}
θ_{max}
40.
35.
30.
25.
20.
15.
10.
5.
0.
-5.
-10.
0.
10.
20.
30.
40.
50.
60.
70.
80.
90.

FIGURE 12

of r_c can dramatically reduce Ψ_{eff}. For example, if $\theta_{max} = 50^o$, $\Psi_{eff} = 14^o$ for $r_c' = 1.5\ r_c$, and $\Psi_{eff} \simeq 10^o$ for $r_c' = 2.0\ r_c$.

We have also calculated η_{ab} and Ψ_{eff} for f/3.5 lenses. An illumination system composed of 20 f/3.5 lenses takes up only 10% of the target solid angle as opposed to 50% for 20 f/1.5 lenses. As Figure 13 indicates, the absorption again does not depart significantly from that at normal incidence, the net absorption at $\theta_{max} = 50^o$ being only slightly inferior to that using f/1.5 lenses. On the other hand, the effective angles of incidence are significantly larger using f/3.5 lenses, as shown in Figs. 14-16. This time the values at $r_c' = 1$, 1.5 and 2.0 are about 25^o, 17.5^o and 12.5^o, resp., all at $\theta_{max} = 50^o$. Since resonant absorption is expected to be strongest for $\Psi = 7\text{-}10^o$, it is apparent that f/3.5 optics exceed this range, even for large expansions of r_c, while f/1.5 optics are marginal, and then only if r_c doubles by the time the bulk of the laser pulse arrives.

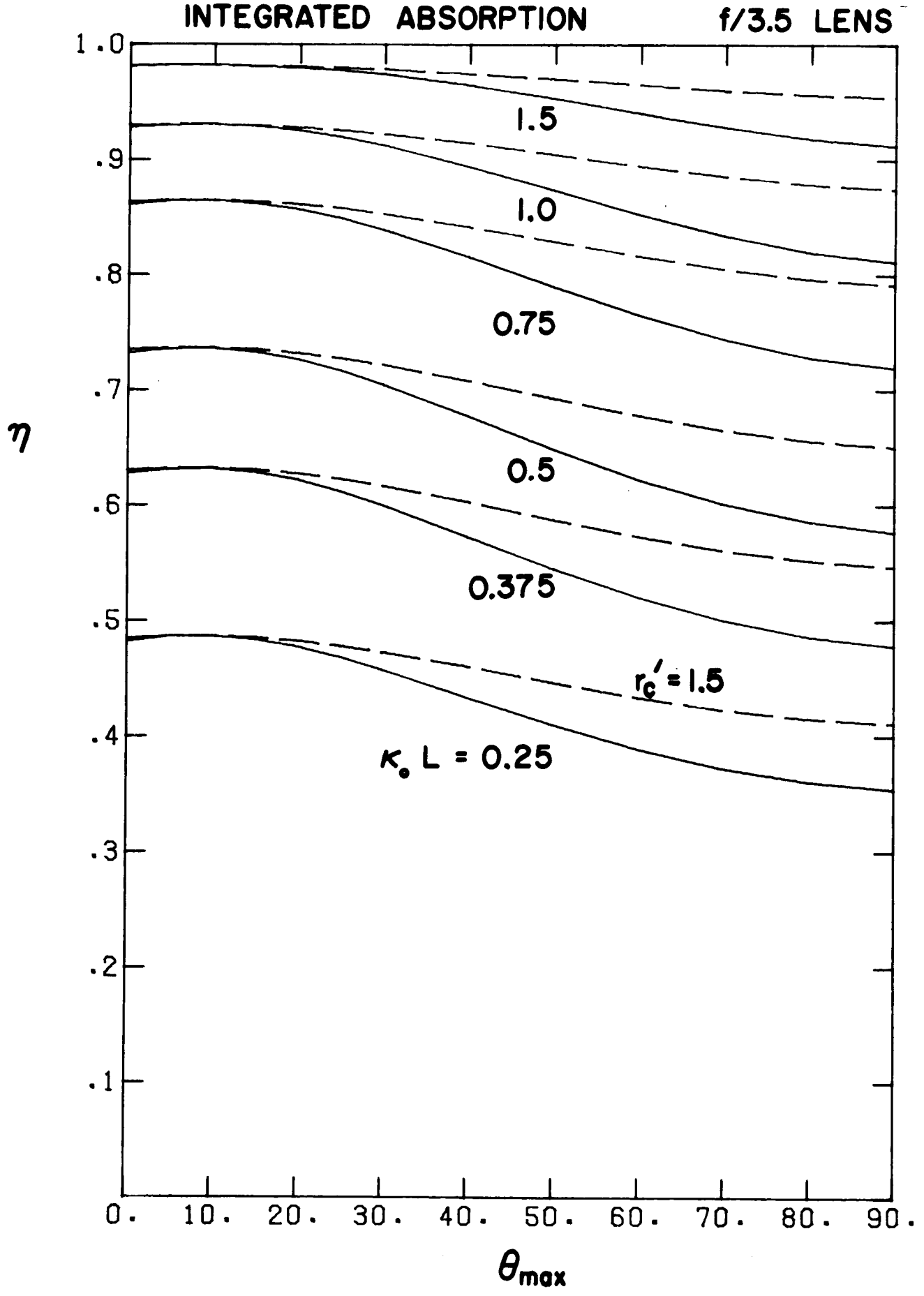
INTEGRATED ABSORPTION
f/3.5 LENS
1.0
.9
.8
.7
.6
.5
.4
.3
.2
.1
η
1.5
1.0
0.75
0.5
0.375
$r_c' = 1.5$
$\kappa_o L = 0.25$
0.
10.
20.
30.
40.
50.
60.
70.
80.
90.
θ_{max}

FIGURE 13

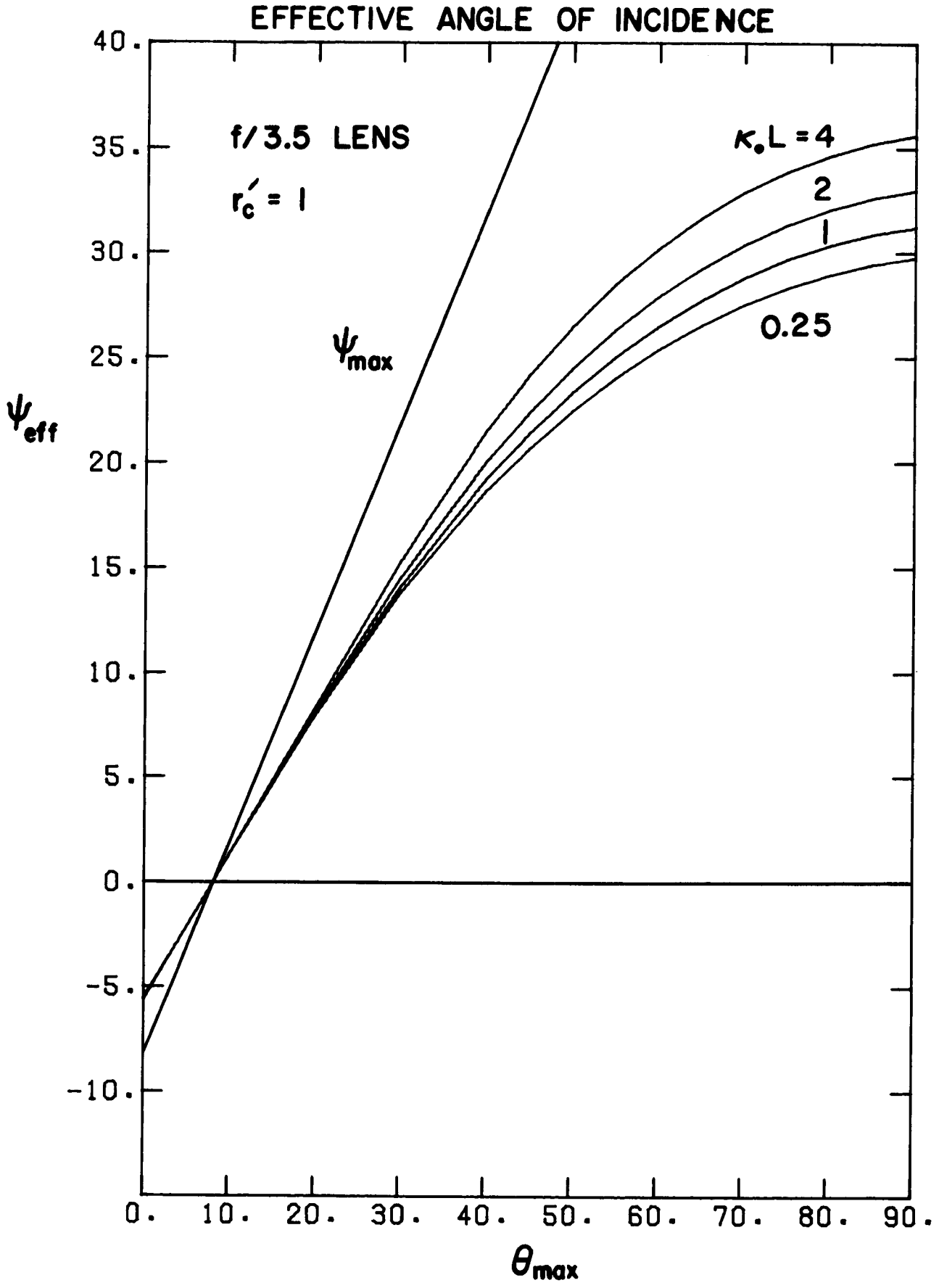
EFFECTIVE ANGLE OF INCIDENCE
f/3.5 LENS
$r_c' = 1$
$\kappa_o L = 4$
2
1
0.25
ψ_{max}
ψ_{eff}
θ_{max}
40.
35.
30.
25.
20.
15.
10.
5.
0.
-5.
-10.
0. 10. 20. 30. 40. 50. 60. 70. 80. 90.

FIGURE 14

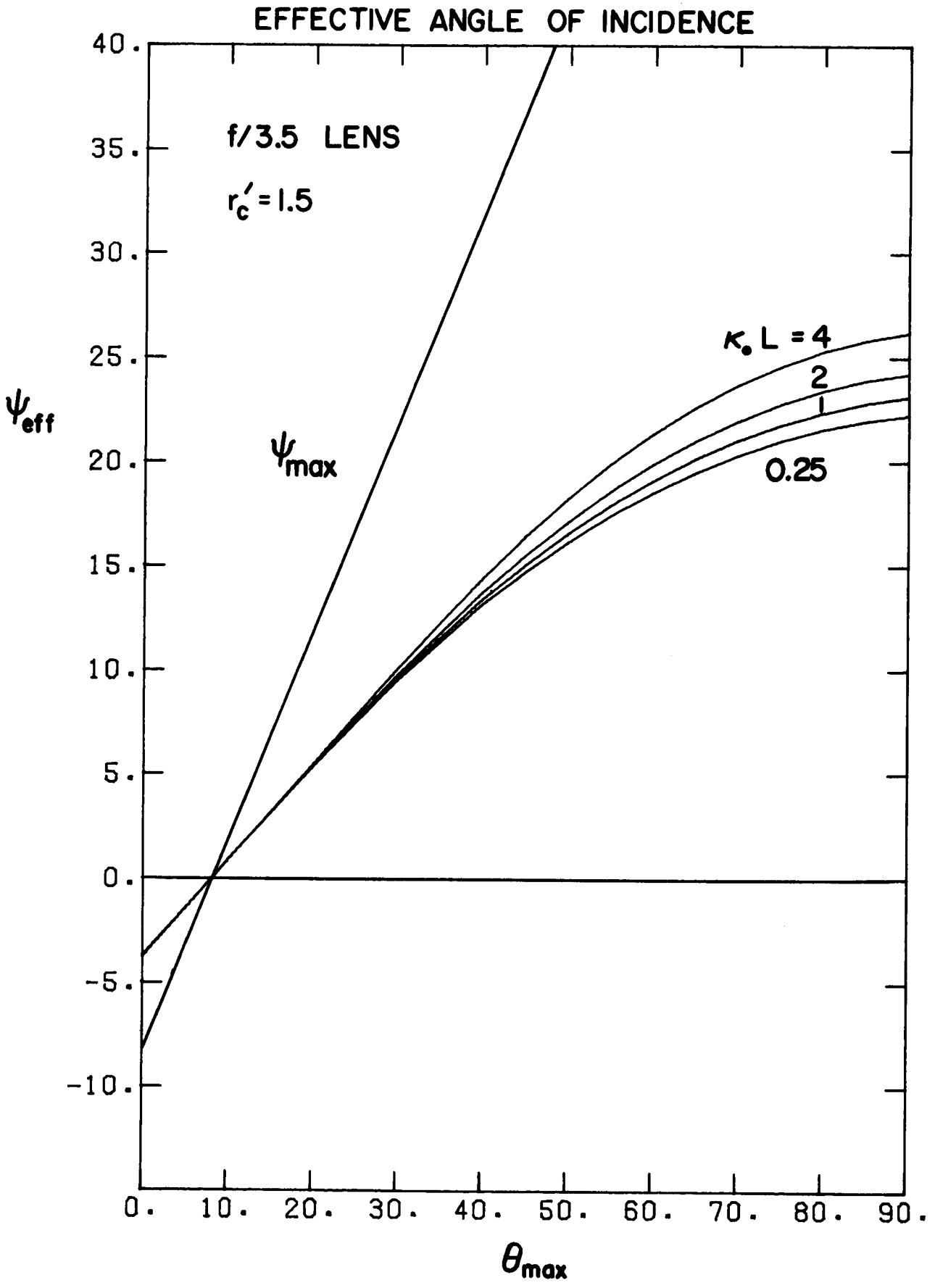
EFFECTIVE ANGLE OF INCIDENCE
f/3.5 LENS
$r_c' = 1.5$
$\kappa_o L = 4$
2
1
0.25
ψ_{max}
ψ_{eff}
θ_{max}
40.
35.
30.
25.
20.
15.
10.
5.
0.
-5.
-10.
0.
10.
20.
30.
40.
50.
60.
70.
80.
90.

FIGURE 15

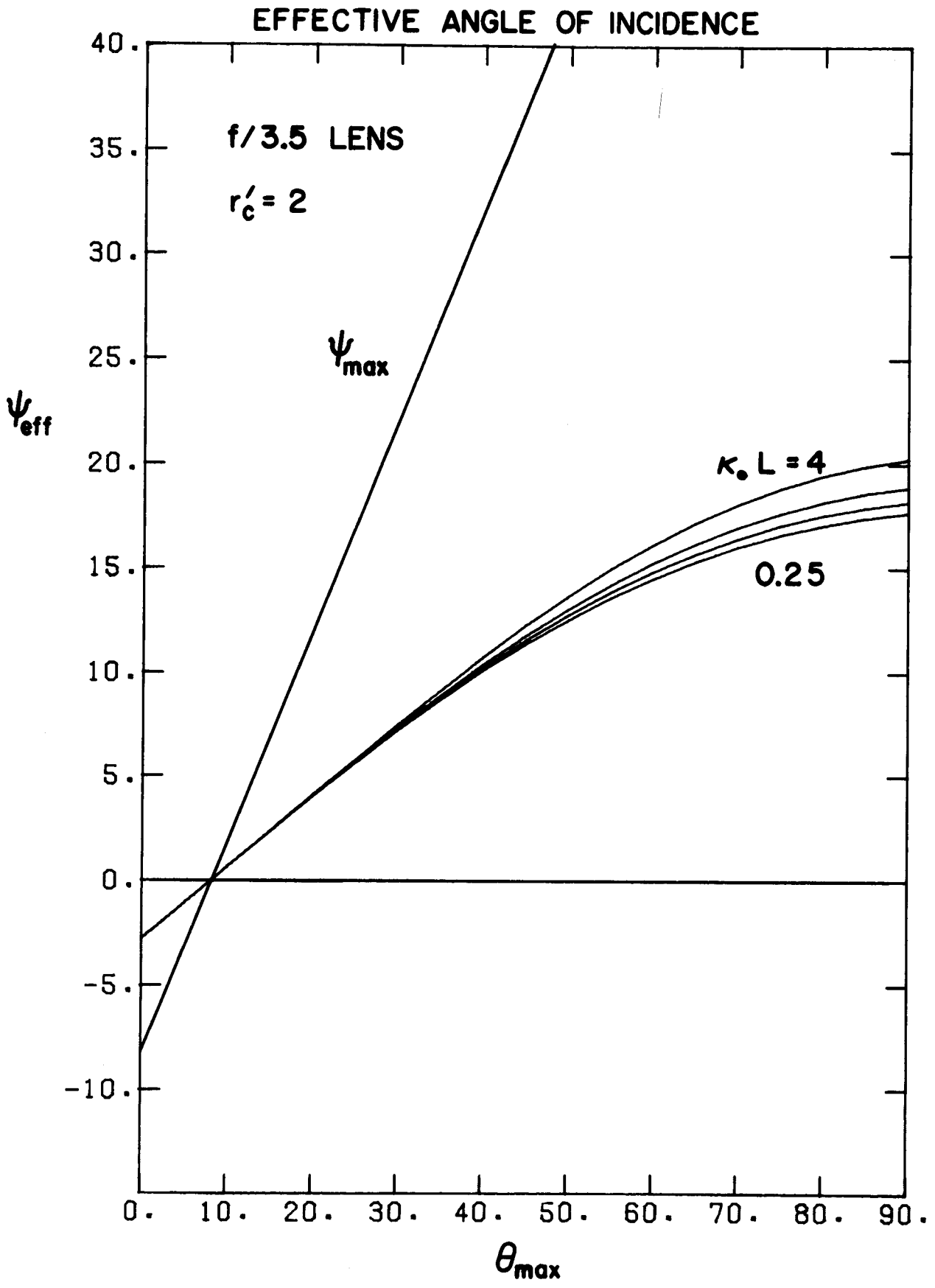
EFFECTIVE ANGLE OF INCIDENCE
f/3.5 LENS
$r_c' = 2$
ψ_{max}
$\kappa_o L = 4$
0.25
ψ_{eff}
θ_{max}
40.
35.
30.
25.
20.
15.
10.
5.
0.
-5.
-10.
0. 10. 20. 30. 40. 50. 60. 70. 80. 90.

FIGURE 16

6. Resonance Absorption and Density Profile Steepening

It is generally acknowledged that nonclassical processes must be invoked to explain the amount of absorption experimentally observed, and required for projected reactor-grade implosions. The prevailing view is that resonance absorption[1] plays a dominant role, the p-polarized component of $\vec{E}$ driving plasma oscillations at the critical surface. A total absorption of over 50% may be obtained in this way.

Resonance absorption is maximized when

$$L\sin^3\theta_0 = \lambda/10.6, \tag{87}$$

where θ_0 is the angle of incidence (our Ψ) and L is the scale height at the critical surface. In the absence of any density profile steepening, strong absorption is confined to a rather narrow range of θ_0. Typical values are 30-50% absorption. Figure 17 shows L as a function of θ_0 for λ = 0.53μm, 1.06μm and 10.6μm. For current experiments on small targets (L = 50-100μm) with λ = 1.06μm, the optimal angle of incidence is seen to be 6-7°, but reactor-grade pellets (L $\cong$ 1000μm) would require $\theta_0 \simeq 3°$. It is difficult to see how such small angles of incidence could be produced under conditions of uniform illumination.

Fortunately, density profile steepening due to radiation pressure, as well as by the resonance absorption process itself,[16] broadens the effective range of incident angles. Extensive numerical studies have been carried out for small pellets, for which scale heights as small as 1μm have been measured.[21] Further numerical simulation is needed to estimate the degree of self-steepening and resonance absorption in the larger pellets envisioned for use in a laser fusion reactor.

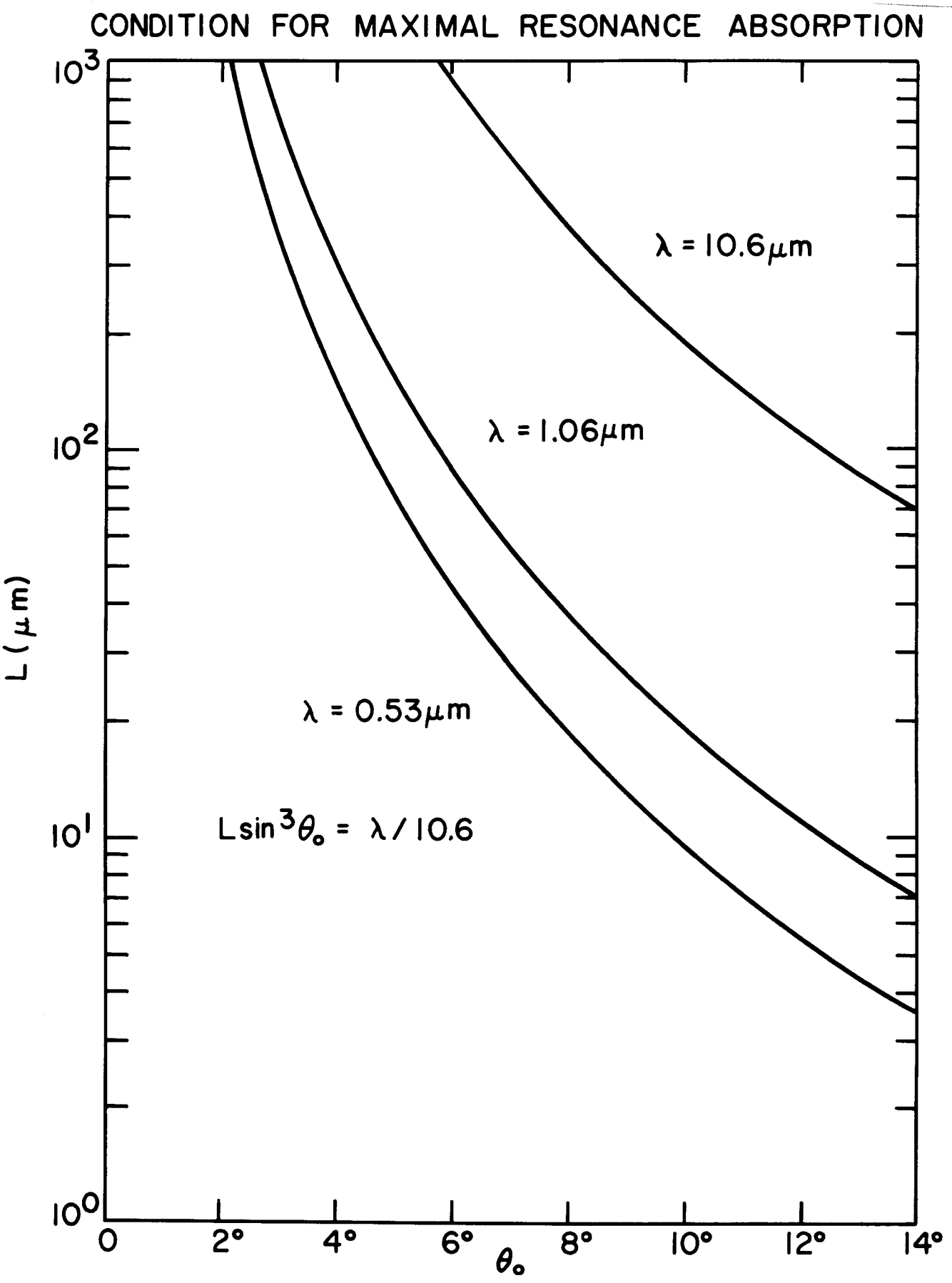
CONDITION FOR MAXIMAL RESONANCE ABSORPTION
10^3
10^2
10^1
10^0
L (μm)
λ = 10.6μm
λ = 1.06μm
λ = 0.53μm
$L\sin^3\theta_o = \lambda / 10.6$
0
2°
4°
6°
8°
10°
12°
14°
θ_o

FIGURE 17

ACKNOWLEDGEMENT

It is a pleasure to thank K. A. Brueckner and H. Brysk for their advice and support in the early phases of this investigation. Able programming assistance was provided by E. Anderson. This research was supported by the Electric Power Research Institute.

REFERENCES

1. J. P. Freidberg, R. W. Mitchell, R. L. Morse and L. I. Rudsinski, Phys. Rev. Lett. 28,795 (1972).

2. H. G. Ahstrom, et. al., Bull. Am. Phys. Soc. 21,1046 (1976).

3. LLL Laser Program Annual Report-1975, UCRL 50021-75, p.307.

4. I. Pelah, E. B. Goldman and B. Yaakobi, Phys. Rev. Lett. 37,829 (1976).

5. R. E. Kidder, Proc. Int. School of Physics (Enrico Fermi) Course 45 (1971).

6. J. E. Howard, R. A. Cover and S. Jorna, Bull. Am. Phys. Soc. 18,1346 (1973).

7. J. N. Shiau, E. B. Goldman and C. I. Weng, Phys. Rev. Lett. 32,352 (1974).

8. S. E. Bodner, Phys. Rev. Lett. 33,761 (1974).
   R. E. Kidder, Nucl. Fusion 16,3 (1976).

9. J. D. Lindl and W. C. Mead, Phys. Rev. Lett. 34,1273 (1975).

10. J. E. Howard, Univ. of Wisconsin Nuclear Engineering Department Report UWFDM-172, 1976.

11. G. Moses, private communication.
    P. Hammerling, private communication.

12. D. W. Forslund, J. M. Kindel and E. L. Lindman, Phys. Fluids 18,1002 (1975).
    LLL Laser Program Annual Report-1975, UCRL 50021-75, p. 311.

13. J. W. Shearer and W. S. Barnes, in Laser Interaction and Related Phenomena, Ed. H. Hora and H. Schwartz, Plenum Press, (New York) 1971.

14. K. A. Brueckner and S. Jorna, Rev. Mod. Phys. 46,325 (1974).

15. J. Dawson, P. Kaw and B. Green, Phys. Fluids 12, 875 (1969).

16. K. G. Estabrook, E. J. Valeo and W.L. Kruer, Phys. Fluids 18,1151 (1975).

17. E. Cojacaru and P. Mulser, Plasma Phys. 17,393 (1975).

18. K. A. Brueckner, private communication.

19. J. W. Shearer, Phys. Fluids 14,183 (1971).

20. M. Born and E. Wolf, Principles of Optics, 2nd ed. Pergamon Press (Oxford) 1964, p. 123.

21. D. W. Phillion and R. L. Lerche, Bull. Am. Phys. Soc. 21,1046 (1976).